Antiviral Research 104 (2014) 40–51

Contents lists available at ScienceDirect

Antiviral Research

journal homepage: www.elsevier.com/locate/antiviral

Molecular modeling and residue interaction network studies on the mechanism of binding and resistance of the HCV NS5B polymerase mutants to VX-222 and ANA598

Weiwei Xue [a], Pingzu Jiao [b], Huanxiang Liu [b], Xiaojun Yao [a,c,*]

[a] State Key Laboratory of Applied Organic Chemistry, Department of Chemistry, Lanzhou University, Lanzhou 730000, China
[b] School of Pharmacy, Lanzhou University, Lanzhou 730000, China
[c] State Key Laboratory of Quality Research in Chinese Medicine, Macau Institute for Applied Research in Medicine and Health, Macau University of Science and Technology, Taipa, Macau, China

ARTICLE INFO

Article history:
Received 12 October 2013
Revised 10 January 2014
Accepted 13 January 2014
Available online 23 January 2014

Keywords:
HCV NS5B polymerase
Mutation-induced drug resistance
Molecular docking
MD simulation
Binding free energy calculation
Residue interaction network

ABSTRACT

Hepatitis C virus (HCV) NS5B protein is an RNA-dependent RNA polymerase (RdRp) with essential functions in viral genome replication and represents a promising therapeutic target to develop direct-acting antivirals (DAAs). Multiple nonnucleoside inhibitors (NNIs) binding sites have been identified within the polymerase. VX-222 and ANA598 are two NNIs targeting thumb II site and palm I site of HCV NS5B polymerase, respectively. These two molecules have been shown to be very effective in phase II clinical trials. However, the emergence of resistant HCV replicon variants (L419M, M423T, I482L mutants to VX-222 and M414T, M414L, G554D mutants to ANA598) has significantly decreased their efficacy. To elucidate the molecular mechanism about how these mutations influenced the drug binding mode and decreased drug efficacy, we studied the binding modes of VX-222 and ANA598 to wild-type and mutant polymerase by molecular modeling approach. Molecular dynamics (MD) simulations results combined with binding free energy calculations indicated that the mutations significantly altered the binding free energy and the interaction for the drugs to polymerase. The further per-residue binding free energy decomposition analysis revealed that the mutations decreased the interactions with several key residues, such as L419, M423, L474, S476, I482, L497, for VX-222 and L384, N411, M414, Y415, Q446, S556, G557 for ANA598. These were the major origins for the resistance to these two drugs. In addition, by analyzing the residue interaction network (RIN) of the complexes between the drugs with wild-type and the mutant polymerase, we found that the mutation residues in the networks involved in the drug resistance possessed a relatively lower size of topology centralities. The shift of betweenness and closeness values of binding site residues in the mutant polymerase is relevant to the mechanism of drug resistance of VX-222 and ANA598. These results can provide an atomic-level understanding about the mechanisms of drug resistance conferred by the studied mutations and will be helpful to design more potent inhibitors which could effectively overcome drug resistance of antivirus agents.

1. Introduction

Hepatitis C virus (HCV), an enveloped single-strand RNA virus, has a major impact on public health. It is estimated that over 3% of the world's population is chronically infected with HCV (Melnikova, 2011). Chronic infection of HCV may lead to cirrhosis and hepatocellular carcinoma and ultimately result in end-stage liver disease and death (D'Oliveira et al., 2009). The standard of care therapy for patients with chronic HCV infection is by using peginterferon (PEG-IFN) with ribavirin, but this associated with frequent and troublesome side effects (Fried, 2002; Fried et al., 2002; Hadziyannis et al., 2004). Fortunately, with the advent of two licensed direct-acting antivirals (DAAs) telaprevir and boceprevir targeting the viral NS3/4A protease in 2011, the treatment outcomes for HCV infection have been greatly improved by the new standard of care, with the combination use of DAAs with PEG-IFN plus ribavirin (De Clercq, 2012; Kanda et al., 2013; Klibanov et al., 2012; Matthews and Lancaster, 2012).

Over the past decades, the knowledge about replication mechanism of HCV has increased tremendously (Lohmann, 2013). This can be particularly reflected by the fact that several

* Corresponding author at: State Key Laboratory of Applied Organic Chemistry, Department of Chemistry, Lanzhou University, Lanzhou 730000, China. Tel.: +86 931 891 2578; fax: +86 931 891 2582.
E-mail address: xjyao@lzu.edu.cn (X. Yao).

http://dx.doi.org/10.1016/j.antiviral.2014.01.006
0166-3542/

crystal structures of the viral enzymes (the NS3/4A protease, the NS3 helicase, the NS5A protein, and the NS5B polymerase) participating in polyprotein processing and replication are available (Bressanelli et al., 1999; Kim et al., 1996; Lesburg et al., 1999; Love et al., 1996; Tellinghuisen et al., 2005; Yao et al., 1999). The results from these studies will be very helpful to the discovery and development on DAAs targeting several important proteins such as NS3/4A, NS5A, or NS5B that are important in the life cycle of HCV (Johnson and Gale, 2006).

HCV NS5B polymerase has been proved to be an important and promising target for anti-HCV drug development and discovery since it has essential functions in viral genome replication. Several nucleoside and nonnucleoside inhibitors (NIs and NNIs) targeting the polymerase has been developed in the advanced stages of clinical development (Soriano et al., 2013). The NNIs interact with one of the four allosteric site (thumb pocket I and II and palm pocket I and II), distinct from the enzyme's active site (Sofia et al., 2011). Among the reported NS5B inhibitors, VX-222 and ANA598 are two promising NNIs in phase II clinical trials (Kirkovsky et al., 2007; Yi et al., 2012). VX-222 is a thiophene-2-carboxylic acid derivative that binds to the thumb II pocket (Figs. 1 and 2). ANA598 (also known as setrobuvir) is a benzothiazidine derivative binding to the palm I pocket (Figs. 1 and 2). However, genotypic mutations resistant to VX-222 (L419M, M423T, and I482L) and ANA598 (M414T, M414L, and G554D) were identified *in vitro* (Kirkovsky et al., 2007; Yi et al., 2012). These resistant mutations

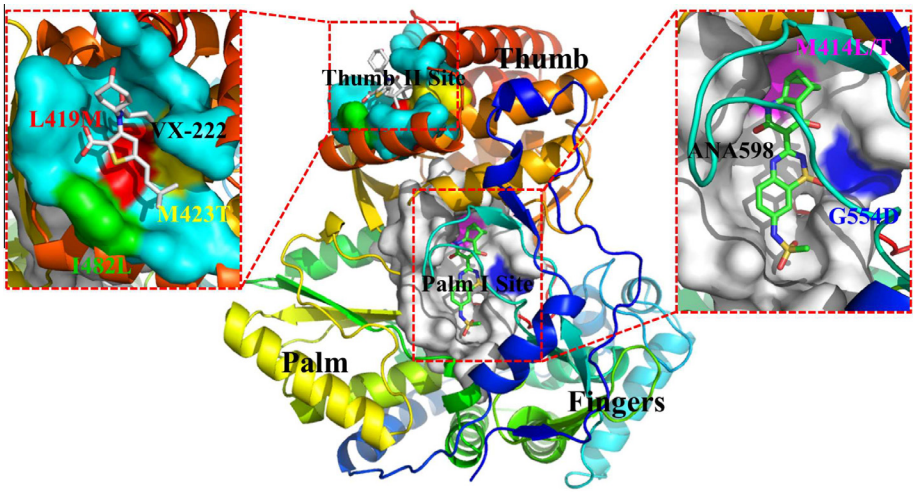

Fig. 1. Structural model of VX-222 and ANA598 bound to the HCV NS5B polymerase thumb II site and palm I site, respectively. The NS5B polymerase is represented in carton and with the thumb II and palm I pocket distinguished in cyan and gray surface. VX-222 and ANA598 are shown in gray and green stick models, respectively. The mutation residues which confer drug resistance are particularly labeled. (For interpretation of the references to color in this figure legend, the reader is referred to the web version of this article.)

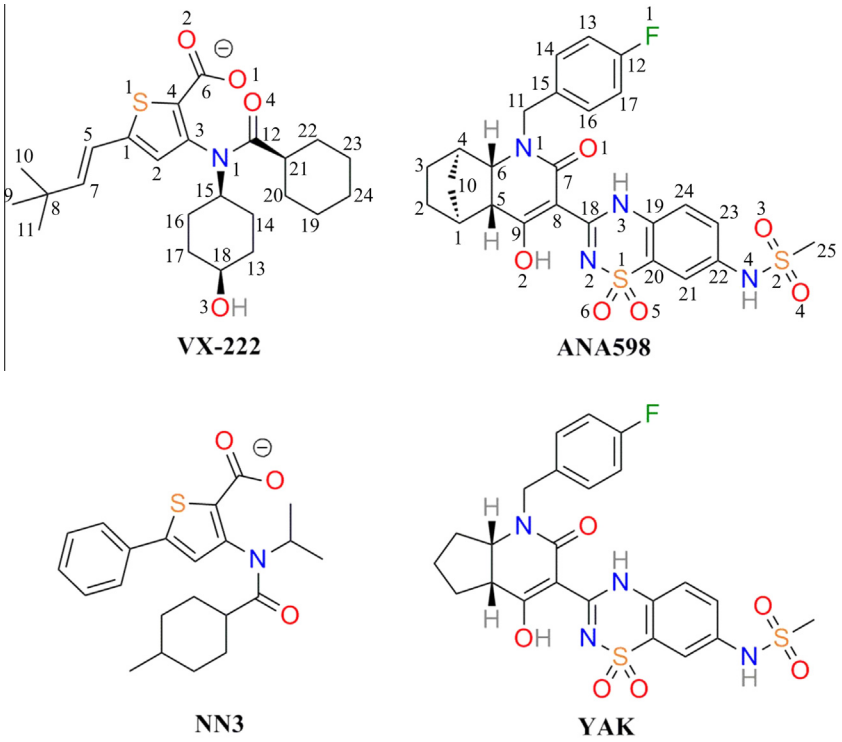

Fig. 2. Chemical structures of VX-222, ANA598, NN3, and YAK. VX-222 and ANA598 are marked up with the atom numbers.

could reduce the potency for VX-222 and ANA598. A detailed understanding of binding and drug resistance mechanism to these two molecules at the atomic level is therefore very crucial for the design of novel potent agents targeting viral variants. Unfortunately, the lack of three-dimensional structures of VX-222 and ANA598 in complex with wild-type and the drug resistant mutants of polymerase has hampered to reveal the molecular basis underlying the binding and resistance mechanism of these two inhibitors. Therefore, elucidating the binding mode and drug resistance mechanism for these two inhibitors from molecular modeling and computational methods could be very valuable.

Molecular modeling and computational methods such as molecular docking, molecular dynamics (MD) simulation, binding free energy calculation, and binding free energy decomposition have been proved to be very useful and successful to provide structural and energetic information to different antiviral agents. Several typical works reported in the past years include the drug resistance mechanism studies against inhibitors to HIV protease, HIV reverse transcriptase (RT), HIV integrase (IN), influenza neuraminidase (NA), HCV NS3/4A protease, and HCV NS5B polymerase (Alcaro et al., 2009; Aruksakunwong et al., 2006; Balius and Rizzo, 2009; Cai and Schiffer, 2010; Chachra and Rizzo, 2008; Guo et al., 2006; Hou et al., 2008; Hou and Yu, 2007; Hou et al., 2009; Jiao et al., 2013; Li et al., 2012; Liu et al., 2010; Pan et al., 2011, 2012; Rizzo et al., 2004; Stoica et al., 2008; Vergara-Jaque et al., 2012; Xue et al., 2013, 2012a,b; Zhang et al., 2010; Zhou et al., 2005). In addition, interactive visualizations of the residue interaction network (RIN) of proteins have been recently devoted to HIV-1 protease, HCV NS3/4A protease, and HIV integrase to gaining insight into complex biological interactions in the mutants systems (del Sol et al., 2006; Welsch et al., 2008, 2012; Xue et al., 2013, 2012a). It is suggested that the resistance mutations in the protein often affect the binding of drugs through influencing the RIN properties of the targets. In a recent publication, the computational investigation by Davis and Thorpe illuminated the allosteric inhibition mechanism of HCV NS5B polymerase (Davis and Thorpe, 2013). This work provides the detailed structure and internal motions of NS5B by an allosteric ligand bound to the thumb domain of the enzyme. However, the binding mode and mutation-induced drug resistance mechanism of VX-222 and ANA598 to the NS5B polymerase were still illusive.

In this work, molecular docking was used to obtain the binding mode of VX-222 and ANA598 to HCV NS5B polymerase. MD simulations were then used to investigate the dynamic interaction mode for VX-222 and ANA598 with wild-type polymerase and its mutants. In addition, the calculated binding free energy and binding free energy decomposition help us to understand the detailed interaction profiles of the VX-222 and ANA598, which can provide important insights into the molecular origins critical to drug resistance. Finally, RIN analysis of the complex can provide some information about the network for the residue interactions to discover the possible mechanisms of drug resistance. These results can provide some potential clues for further design of novel inhibitors that are less susceptible to drug resistance.

2. Materials and methods

2.1. Initial models preparation

The initial coordinates of wild-type (WT) crystal structures for the polymerase were derived from the Protein Data Bank (PDB ID code: 2GIR (Le Pogam et al., 2006) and 3H2L (Ruebsam et al., 2009)), only one monomer was retained. The structures of VX-222 and ANA598 were modified with the Maestro (Schrödinger, 2009a) building tools based on the ligands, NN3 and YAK (Fig. 2), extracted from the crystal structures of 2GIR and 3H2L, respectively. The build inhibitors VX-222 and ANA598 were then preprocessed by the LigPrep (Schrödinger, 2009b) which uses OPLS-2005 force field (Kaminski et al., 2001) and gave the corresponding low energy 3D conformers of the compounds. The ionized state was assigned by using the Epik (Schrödinger, 2009c) at a target pH value of 7.0 ± 2.0. As for the polymerase structures, the missing loop region of the encompassing residues 149–153 in 2GIR and 3H2L were predicted and refined with Prime (Schrödinger, 2009d). The Protein Preparation Wizard in Maestro was used to remove crystallographic water molecules, add hydrogen atoms, assign partial charges and protonation states, and minimize the structures. The minimization was terminated when the root-mean-square deviation (RMSD) reached a maximum value of 0.30 Å.

Subsequently, molecular docking was used to study the binding mode of VX-222 and ANA598 to HCV NS5B polymerase. The prepared VX-222 and ANA598 structures were respectively docked into the NN3 and YAK binding site of the minimized polymerase using the Glide (Schrödinger, 2009e) with the standard precision (SP) scoring mode. The docking grid boxes for VX-222 and ANA598 were defined by centering on the NN3 and YAK in the polymerase, respectively. In molecular docking, 5000 poses were generated during the initial phase of the docking calculation, out of which best 1000 poses were chosen for energy minimization by 1000 steps of conjugate gradient minimizations. Finally, molecular docking gave 4 and 9 poses, respectively for ligands VX-222 and ANA598 bound to the polymerase (Supplementary Figs. S1 and S2). We selected the best binding poses for further study (Supplementary Fig. S3). On the basis of the docked models of VX-222 and ANA598 in complex with wild-type polymerase, we also constructed the models for the studied mutant complexes by substituting the specific residues of wild-type polymerase (L419M, M423T, and I482L for VX-222 and M414L, M414T, and G554D for ANA598). All the molecular modeling calculation process was carried out with the Schrödinger software.

2.2. Parametrization of ligands

The force field parameters for VX-222 and ANA598 were described by the General AMBER Force Field (GAFF) (Wang et al., 2004) and Restrained Electrostatic Potential (RESP) (Bayly et al., 1993; Cieplak et al., 1995; Fox and Kollman, 1998) partial charges. Geometry optimization and the electrostatic potential calculations were performed at the HF/6-31G* level of Gaussian09 suite (Frisch et al., 2009).

2.3. MD simulations

Each system was neutralized with chloride ions and was solvated in a rectangular pre-equilibrated TIP3P (Jorgensen et al., 1983) water box. Sufficient solvent was added to provide a minimum distance of 10 Å between any protein atom and the edge of the box. This yielded a simulation box containing approximately 18500 water molecules with initial dimensions of $87 \times 90 \times 99$ Å^3.

All systems were energy minimized and equilibrated using the AMBER10 (Case et al., 2008) with the standard AMBER03 force field (Duan et al., 2003) and TIP3P water model. First, each system was minimized using steepest descent method for 3000 steps followed by conjugated gradient method for 2000 steps. During the minimization, the harmonic restraints with a force constant of 500.0 kcal/(mol · Å^2) were applied for all protein atoms. Further minimization are carried out with all atoms relax for 3000 steps using steepest descent method followed by 2000 steps of conjugated gradient method. The systems were sequentially heated up from 0 to 310.0 K over 100 ps in the *NVT* ensemble and equilibrating to adjust the solvent density under 1 atm

pressure over 50 ps in the *NPT* ensemble simulation by restraining all protein atoms of the structures with a harmonic restraint weight of 10.0 kcal/(mol · Å^2). An additional three molecular dynamics equilibrations of 50 ps each were performed with the decreased restraint weights of 5.0, to 1.0, to 0.1 kcal/(mol · Å^2), respectively. These were followed by unconstrained 50 ps of equilibration at 310.0 K.

MD simulations production was carried out without any restraint on these eight systems in the *NPT* ensemble at a temperature of 310.0 K and a pressure of 1 atm. During the simulations, periodic boundary conditions were employed and direct space interactions were truncated at a distance 10.0 Å with long range contributions from the electrostatics included using the particle mesh Ewald (PME) method (Darden et al., 1993). All bonds involving hydrogen atoms were constrained with the SHAKE algorithm (Ryckaert et al., 1977), allowing an integration time step of 2 fs. The coordinates of the trajectories were saved every 1 ps for analysis.

2.4. Thermodynamic analysis

Binding free energy (ΔG_{bind}) for the inhibitors VX-222 and ANA598 to HCV NS5B polymerase was calculated using the MM/GBSA method (Kollman et al., 2000; Massova and Kollman, 2000; Onufriev et al., 2000; Tsui and Case, 2000), as reported previously (Xue et al., 2013, 2012a). The MM/GBSA binding free energy, which consists of an electrostatic, van der Waals, polar, nonpolar, and entropic component. The electrostatic (ΔE_{ele}) and van der Waals (ΔE_{vdW}) contributions are computed using the molecular mechanics energy function. The polar contributions (ΔG_{GB}) were calculated by solving the GB equation, with dielectric constants for solute and solvent set to 1 and 80, respectively (Rocchia et al., 2001). The nonpolar contributions (ΔG_{SA}) were estimated by the solvent-accessible surface area (SASA) determined using a water probe radius of 1.4 Å and the surface tension constant γ was set to 0.0072 kcal/(mol/Å^2) (Sitkoff et al., 1994). The solute entropy change ($-T\Delta S$) were estimated by normal mode analysis (Pearlman et al., 1995). In this work, a single trajectory approach is carried out for the protein–ligand complex. The MM/GBSA binding free energy and per-residue binding free energy decomposition were determined by extracting 1000 snapshots at 10 ps interval from the last equilibrated 10 ns trajectory of the simulation for each complex. Due to the high computational cost in the entropy calculation, 100 snapshots were used to normal mode analysis.

2.5. Residue interaction network analysis

In order to construct the RIN interactively in 2D graphs, the representative structures derived from the last 10 ns trajectory of each system was used. First, REDUCE (Word et al., 1999b) was applied for accurately adding hydrogen atoms to the protein structure. Then, the noncovalent interaction residues between the atoms of each pair of considered residues were identified by PROBE (Word et al., 1999a). Finally, Cytoscape (Shannon et al., 2003) and the plugin RINalyzer (Doncheva et al., 2011) were used to visualize the network. In a RIN, the nodes represent the protein residues and the edges between them represent the noncovalent interactions.

To highlight and investigate the similarities and differences between the networks corresponding to wild-type and the mutant polymerase, we generated a combined comparison network of two RIN using RINalyzer based on the superposition alignment of the corresponding 3D structures. The comparison network contains different types of edges and nodes according to the preserved residue interactions and the aligned residues.

In this work, we also performed the protein topological parameters analysis of shortest path betweenness and closeness centrality by using the NetworkAnalyzer (Assenov et al., 2008) plugin of Cytoscape. The betweenness centrality of a node reflects the amount of control that this node exerts over the interactions of other nodes in the network (Yoon et al., 2006), whereas the closeness centrality is a measure of how quickly information spreads from a given node to other reachable nodes in the network (Freeman, 1978).

3. Results and discussion

3.1. Binding mode of VX-222 and ANA598 to NS5B polymerase by molecular docking

Since VX-222 and ANA598 are derivatives of the first class NS5B inhibitors NN3 and YAK (Fig. 2) cocrystallized with the thumb II and palm I domain of HCV NS5B polymerase (PDB ID code: 2GIR (Le Pogam et al., 2006) and 3H2L (Ruebsam et al., 2009)), respectively, these two crystal structures of NS5B polymerase were selected in our molecular docking studies. Supplementary Figs. S1 and S2 depict the superimposition for the docking poses of VX-222 and ANA598 with the crystal structures NN3 and YAK, respectively. We can see from Supplementary Fig. S1 that all of the obtained VX-222 docking poses are similar to NN3 structure in 2GIR. Meanwhile, the docking poses of ANA598 in Supplementary Figs. S2A–S2E are similar to YAK in 3H2L, however, there are some difference in Supplementary Figs. S2F–S2I. Overall, we noticed that Supplementary Figs. S1A and S2A show the most similar poses and were considered for the further analysis (Fig. 1 and Supplementary Fig. S3).

As shown in Fig. 1, the build models of VX-222 binds to the thumb II allosteric pocket and ANA598 binds to the palm I allosteric pocket. In detail, VX-222 binding with the pocket characterized by residues L392, L419, M423, R422, L474, H475, S476, Y477, I482, V485, L497, R527, and W528 (Supplementary Fig. S3A). As for ANA598, the pocket consists of F193, P197, R200, D225, S267, T287, S288, N291, N316, D318, D319, C366, L384, S407, N411, M414, Y415, Q446, Y448, G554, and S556 (Supplementary Fig. S3B). Moreover, these two binding sites are consistent well with the mutations identified in clinical trials that confer drug resistance (Kirkovsky et al., 2007; Yi et al., 2012). Therefore, on the basis of these two models, we obtained the binding mode of VX-222 and ANA598 in the mutant polymerase. However, to get more deep insight into the mode of binding and the influence of the resistance mutations on the drug binding, we performed additional MD simulations and binding free energy calculation on these build models.

3.2. Stability of the polymerase–inhibitor complexes during the MD simulations

A total of 240 ns MD simulation were conducted in explicit aqueous solution for two wild-type and six drug-resistant mutants (L419M, M423T, and I482L for VX-222 and M414T, M414L, and G554D for ANA598) complexes. To monitor the convergence of the each trajectory, the RMSD of each snapshot relative to the initial structure was calculated. Fig. 3 and Supplementary Figs. S4 and S5 depict the RMSD plots for protein backbone atoms, the backbone atoms of protein residues around 5 Å of ligand as well as ligand heavy atoms with respect to the initial structure as a function of time. The distributions of these RMSD values indicate that all systems have reached equilibrium in the MD simulations. As observed in Fig. 3, the RMSD for the protein backbone atoms of the complexes of VX-222 bound to WT, L419M, M423T, and I482L polymerase in the simulation fluctuates around 1.7, 1.6, 1.4 and 1.5 Å after 5 ns (Fig. 3A), and this fluctuates around 2.0, 2.0,

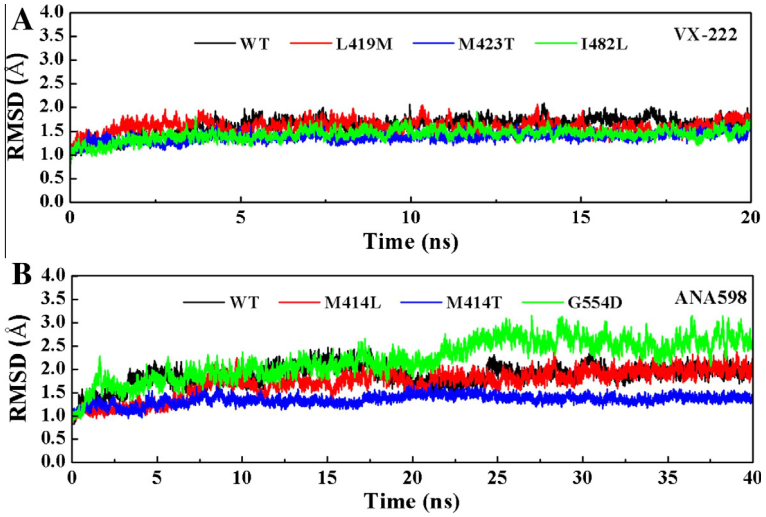

Fig. 3. The backbone atom RMSD for (A) VX-222 and (B) ANA598 bound wild-type and mutant polymerase, calculated with respect to the initial structure during the MD simulation.

1.4 and 2.6 Å after 30 ns in the complexes of ANA598 bound WT, M414L, M414T, and G554D polymerase (Fig. 3B). It is notable that there are relatively large fluctuations of the G554D mutant complexes. This can been explained by the previous studies that tampering with the 531–570 region can destabilize the closed thumb form of the polymerase (Adachi et al., 2002). Recently, the study by Davis and Thorpe provides the first evidence for a mechanistic basis of allosteric inhibition in NS5B polymerase using MD simulations based on X-ray crystal structure (Davis and Thorpe, 2013). However, the simulation structures took about 100 ns in reaching equilibration due to a general conformational change. This is due to the initial structure used by the authors with a slightly more open thumb (PDB ID code: 2WHO (Ontoria et al., 2009)) than the structures used in this work (PDB ID code: 2GIR (Le Pogam et al., 2006) and 3H2L (Ruebsam et al., 2009)). The structure 2WHO being deleted of 60 C-terminal NS5B polymerase residues instead of just 21 in 2GIR and 3H2L. That further deletion is known to induce an opening of NS5B polymerase thumb (Adachi et al., 2002; Caillet-Saguy et al., 2011).

3.3. Comparison of the binding mode of inhibitors with wild-type and mutant polymerase structures

Fig. 4 illustrates the detailed structural comparison of the representative structures for VX-222 and ANA598 in complex with wild-type and mutant polymerase. The representative structure of each complex is from their conformational ensemble using the average structure of the last 10 ns equilibrated trajectory. As shown in Fig. 4 A–C, VX-222 binds to the polymerase mainly through hydrophobic and hydrogen bond contacts. The acid group of VX-222 forms hydrogen bond interactions with the main chain of S476 and Y477. The neohexyl and the cyclohexyl groups of VX-222 interact with the hydrophobic binding pocket formed by residues L419, M423, I482, and L497. The overall orientation of VX-222 in the thumb II binding pocket of mutant polymerase remained all key interactions in wild-type polymerase (Fig. 4A–C). In the case of ANA598 binding to the polymerase palm I pocket (Fig. 4D–F), we noticed that the 4-fluorobenzyl and exo-bicyclic moieties of ANA598 formed strong hydrophobic interactions with P197, C366, M414, Y415, and I447. Hydrogen bond was also observed between the oxygen atoms of the benzothiadiazin group and the side chain of Q446.

In Fig. 4, we can also find that there are some difference between the conformational features of wild-type and mutant polymerase upon VX-222 and ANA598 binding. Comparison of these two systems, the ANA598 bound mutant complexes seems to undergo more conformation changes (Fig. 4D–F). Here, by using the structure in wild-type complex as a reference, the RMSD values for the heavy atoms of VX-222 are 1.19, 1.48, and 1.36 Å in L419M, M423T, and I482L mutant complexes, respectively. The RMSD values for the heavy atoms of ANA598 are 4.27, 3.19, and 2.73 Å in M414L, M414T, and G554D mutant complexes. As can be seen from Fig. 4, the orientations changes of the VX-222 and ANA598 in the mutant polymerase is mainly because of the bulky side chain of the mutant residues which has an unfavorable steric contact with the drugs. Additionally, the binding pocket residues of the polymerase mutants also undergo some conformation change to accommodate the VX-222 and ANA598 (Fig. 4). To quantify these conformational changes of the polymerase binding site induced by mutations and inhibitors binding, we first examined the RMSD of the atoms of the key residues in the VX-222 and ANA598 binding pocket with respect to wild-type structure. The calculated RMSD are 3.91, 4.36, and 1.27 Å for VX-222 bound L419M, M423T, and I482L mutant complexes, and 3.97, 4.20, and 3.33 Å for ANA598 bound M414L, M414T, and G554D mutant complexes. The large value of RMSD indicates that the obvious conformational changes have been identified for the key residues. Subsequently, to assess the local structural transformations of polymerase in more detail, the root mean squared fluctuations (RMSF) of each residue during MD simulation depicted in Fig. 5 was computed. The RMSF analysis on the polymerase indicated that the fluctuations of the residues in the mutant are higher than the VX-222 and ANA598 bound wild-type polymerase. This means that the conformational flexibility of the mutant polymerase is actually large to allow inhibitors binding, but interaction between the drugs and mutants is weakened due to the conformation changes.

3.4. Hydrogen bonds between polymerase and drugs

Further analysis on the representative structures of the drug–polymerase complexes (Fig. 4) suggests that hydrogen bonds may play an important role to stabilize the interaction between the polymerase and the two drugs. In the drug bound wild-type polymerase complexes, VX-222 forms hydrogen bonds with the main chain of S476 and Y477, whereas ANA598 forms hydrogen bonds with the side chain of Q446 (Fig. 4). Fig. 4A–C demonstrated that VX-222 forms similar hydrogen bond network with the mutant polymerases. In contrast, ANA598 has hydrogen

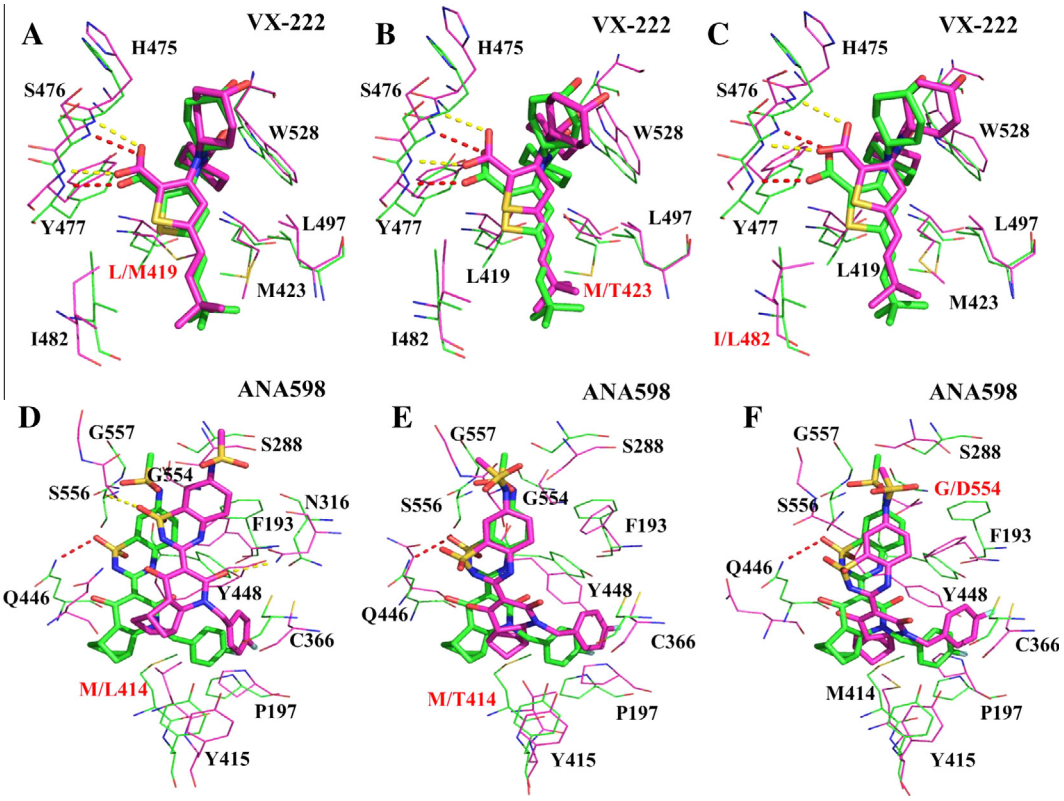

Fig. 4. Superimposition of the (A) VX-222 and (B) ANA598 bound wild-type and mutant complexes, The line representations are shown for wild-type (green) and the mutant (pink) polymerase residues in the drugs binding pocket. VX-222 and ANA598 are shown as a stick representation in wild-type (green) and the mutant (pink) models. (For interpretation of the references to color in this figure legend, the reader is referred to the web version of this article.)

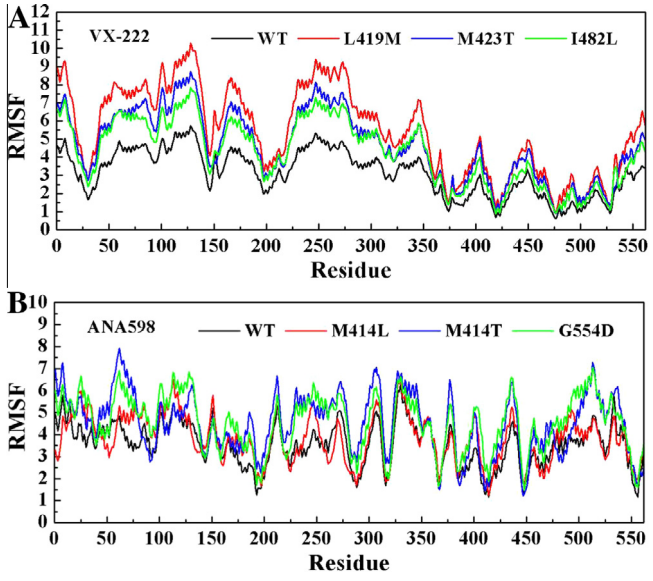

Fig. 5. RMSF of Cα for (A) VX-222 and (B) ANA598 bound wild-type and mutant polymerase averaged over the simulation.

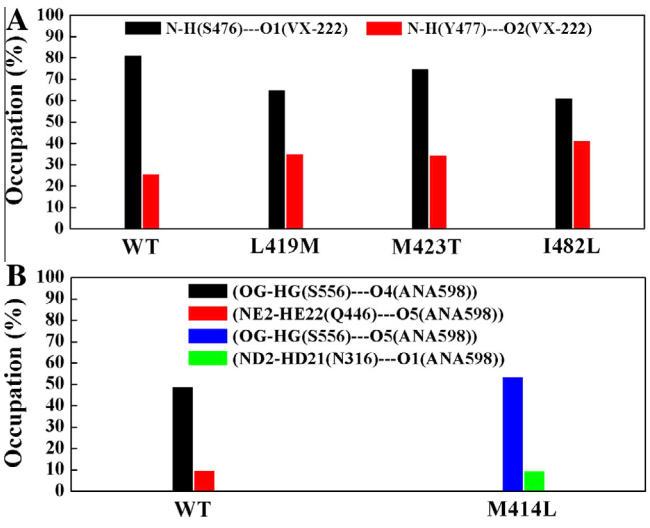

Fig. 6. Monitoring for the intermolecular hydrogen bonds between the polymerase and ANA598 during the MD simulation. (A) Percentage of hydrogen bond occupancy between VX-222 and the polymerase for wild-type and mutant polymerase complexes. (B) Percentage of hydrogen bond occupancy between ANA598 and the polymerase for wild-type and mutant models.

bonding interaction with N316 and S556 in the M414L mutant. Additionally, ANA598 hardly forms hydrogen bond with N316, Q446, or S556 in the M414T and G554D mutants. Herein, to further investigate how drug resistance mutations influence on the hydrogen bonds interaction, we examined the hydrogen bonds network in the eight systems. The percentages of hydrogen bonds during the MD simulations were calculated and the results were displayed in Fig. 6. As can be seen from Fig. 6A, the hydrogen bond occupancies of VX-222 with S476 (N–H(S476)···O1(VX-222)) in wild-type and the L419M, M423T, and I482L mutant polymerase are 81.41%, 65.15%, 75.14%, and 61.41%, respectively, indicating that the drug resistant mutations weaken the hydrogen bond interaction between VX-222 and S476. The hydrogen bond interaction between VX-222 and Y477 (N–H(Y477)···O2(VX-222)) are increased in all three mutant complexes (Fig. 6A). In addition, the

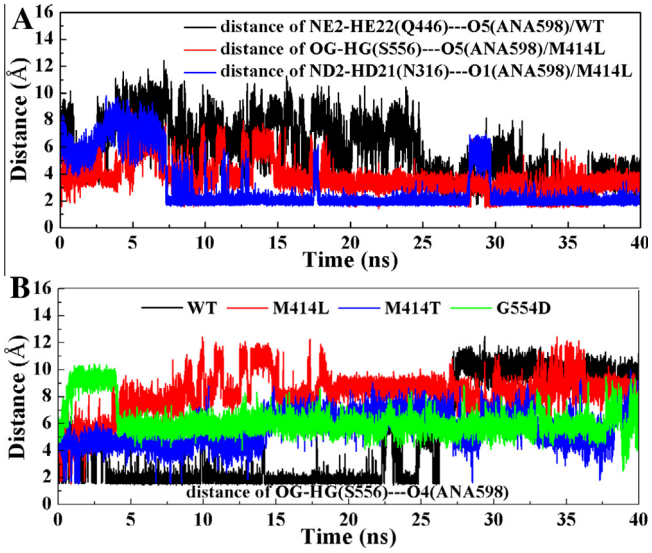

Fig. 7. Monitoring for the intermolecular hydrogen bonds between the polymerase and ANA598 during the MD simulation. (A) The time evolution of hydrogen bond distance of (NE2-HE22(Q446)···O5(ANA598) for the ANA598 bound wild-type and HG(S556)···O5(ANA598) and HD21(N316)···O1(ANA598) for the ANA598 bound M414L mutant polymerase complexes. (B) The time evolution of hydrogen bond distance of HG(S556)···O4(ANA598) for the ANA598 bound wild-type and mutant polymerase complexes.

distance between the donor and acceptor atoms of the above two hydrogen bonds in wild-type and mutant complexes remains relatively stable during the simulation (Supplementary Fig. S6).

In Fig. 6B, we found that the occupancy of the hydrogen bond between ANA598 and Q446 (NE2-HE22(Q446)···O5(ANA598) was 9.98% in wild-type polymerase. The distance between the donor and acceptor atoms shown in Fig. 7A revealed that this important hydrogen bond formed after about 25 ns MD simulation. In addition, ANA598 has hydrogen bond interaction with S556 ((OG-HG(S556)···O4(ANA598), 49.03%) in wild-type polymerase, but this hydrogen bond interaction disappeared when the hydrogen bond between ANA598 and Q446 formed, this may be explained by the calculated distance between the donor and acceptor atoms during the MD simulations shown in Fig. 7B. The hydrogen bond interaction change in ANA598 bound wild-type complex is also consistent with the ligand conformational change after about 25 ns MD simulation (Supplementary Fig. S5B). In all three mutant complexes, the O4 atom of ANA598 hardly forms hydrogen bond with S556 during the simulation (Fig. 7B). However, in the M414L mutant complex, ANA598 has hydrogen bond interaction with N316 ((OG-1HD2(N316)···O1(ANA598), 53.90%) and S556 ((OG-HG(S556)···O5(ANA598), 9.85%) (Fig. 6B), and the evolution of distance between the donor and acceptor atoms during the simulation is shown in Fig. 7A.

3.5. The difference of the binding free energy between the drugs with wild-type and mutant polymerase

3.5.1. Total binding free energy decreases caused by resistance mutations

The influence of drug resistance mutations on binding free energy (ΔG_{bind}) between the drugs and polymerase was evaluated for the eight complexes. Table 1 summarizes the detailed contribution of various energy components based on MM/GBSA method. As shown in Table 1, the calculated ΔG_{bind} for VX-222 binding to wild-type and the L419M, M423T, and I482L mutant polymerase are −14.56, −10.60, −10.87, and −11.65 kcal/mol, respectively. Compared with wild-type complex, mutant complexes have lower binding free energy. This suggests that VX-222 bind less strongly to all three mutant polymerase than that of wild-type polymerase. For ANA598 binding to wild-type and the M414L, M414T, and G554D mutant polymerase, the binding free energy are −12.15, −9.95, −5.06, and −4.58 kcal/mol, which is in a reasonable agreement with the experimental measurements. Herein, to better compare the experimental and theoretical results, the calculated dissociation constant K_d, experimental EC_{50} (Kirkovsky et al., 2007; Yi et al., 2012), and their fold increase for VX-222 and ANA598 bound to wild-type and mutant polymerase are given in Table 2. The result shown in Table 2 indicates that the calculated K_d fold increase follow consistently the order of the experimental EC_{50} fold increase for ANA598 bound complexes. However, there are some differences between the theory and experimental fold increase for VX-222 bound complexes.

In addition, to better understand the binding mechanisms, we provide the individual contributions to the binding free energy. Here, the calculated contributions favoring to the binding include electrostatic energy (ΔE_{ele}), intermolecular van der Waals energy (ΔE_{vdW}), and nonpolar solvation energy (ΔG_{SA}), whereas polar solvation energy (ΔG_{GB}) has unfavorable contribution to the binding process (Table 1). Besides, estimation of the corresponding entropic contributions ($-T\Delta S$) upon binding of VX-222 and ANA598 to wild-type and mutant were carried out for the purpose of predict the ΔG_{bind} more accurately. The calculated binding entropy ($-T\Delta S$) shown in Table 1 indicate that conformational change plays an important role to the polymerase–inhibitors interaction. Moreover, these entropy changes, ranging from 18.43 to 22.06 kcal/mol, have unfavorable values to the total binding free energies.

3.5.2. Interaction energy change for individual residues caused by resistance mutations

In order to gain insight into the residues responsible for the loss of binding affinity conferred by drug resistant mutations, the contribution of each residue to the binding was calculated for both wild-type and mutant polymerase (Supplementary Figs. S7 and S8), and their differences are shown in Figs. 8 and 9. On the basis of the

Table 1
The calculated binding free energies for VX-222 and ANA598 bound to wild-type and mutant polymerase based on MM/GBSA method.

System		Contribution [a]						
		ΔE_{ele}	ΔE_{vdW}	ΔG_{SA}	ΔG_{GB}	ΔE_{bind}	$-T\Delta S$	ΔG_{bind} [b]
VX-222	WT	−300.53	−40.47	−4.83	311.59	−34.24	19.68	−14.56
	L419 M	−297.57	−36.84	−4.42	307.31	−31.52	20.92	−10.60
	M423T	−292.64	−35.85	−4.44	301.47	−31.46	20.59	−10.87
	I482L	−312.21	−38.81	−4.73	322.04	−33.71	22.06	−11.65
ANA598	WT	−7.88	−52.40	−6.33	36.03	−30.58	18.43	−12.15
	M414L	−17.11	−54.45	−6.83	49.78	−28.61	18.66	−9.95
	M414T	−38.84	−48.35	−6.16	67.49	−25.86	20.80	−5.06
	G554D	−35.93	−44.79	−5.96	63.73	−22.95	18.37	−4.58

[a] All energies are in kcal/mol.
[b] $G_{bind} = \Delta E_{bind} - T\Delta S$.

Table 2
The calculated K_d, experimental EC_{50}, and their fold increase for VX-222 and ANA598 bound to wild-type and mutant polymerase.

Systems	VX-222				ANA598			
	WT	L419M	M423T	I482L	WT	M414L	M414T	G554D
K_d[a] ($\times 10^{-10}$)	0.2	172.6	109.5	29.4	12.6	516.6	1969400.1	4424453.1
K_d fold increase	1	863	547.5	147	1	41	156301.6	351147.1
EC_{50} (nM) [b]	5.2	45.3	79.8	563.1	0.5	298	468	634
EC_{50} fold increase	1	8.7	15.3	108.3	1	596	936	1268

[a] K_d was derived from the calculated ΔG_{bind} values in Table 1 by using the equation $\Delta G_{bind} = RT\ln K_d$.
[b] EC_{50} is derived from the experimental values in the references Kirkovsky et al. (2007), Yi et al. (2012).

decomposed interaction energy, we found that S476, H475, W528, L419, L497, Y477, I482, M423, and L474 are important for VX-222 binding, and the contributions are −4.56, −3.94, −2.88, −2.65, −1.90, −1.85, −1.54, −1.41, and −0.63 kcal/mol, respectively (Supplementary Fig. S7). Meanwhile, the contributions of individual residues to the binding of ANA598 can be ranked as follows: Y448 > Q446 > Y415 > M414 > S556 > G557 > F193 > S288 > P197 > C366 > N411 > L384 > S368 > G554 (Supplementary Fig. S8).

In VX-222 bound three mutant complexes, the contribution from the residues M419, L423, and L482 are decreased by 0.43, 0.67, and 0.18 kcal/mol, respectively (Fig. 8). For the other residues including L474, H475, S476, Y477, L497, and W528, the mutations also influenced the interaction energies. Among those residues, L474, H475, S476, L497, and W528, are related to the contribution decrease of VX-222 interaction with the important residues, whereas the interaction energy for the Y477 increased. Specifically, the increase in the interaction energy for Y477 is mainly because of the enhanced hydrogen bond interaction between VX-222 and Y477 in the mutant models as mentioned above (Fig. 6A). Furthermore, by comparing the total polar contributions and the total nonpolar contributions presented in Supplementary Fig. S9, we observed that the main contribution loss of the residues was from the nonpolar interaction energy and the favorable contributions of Y477 are from the polar interaction energy.

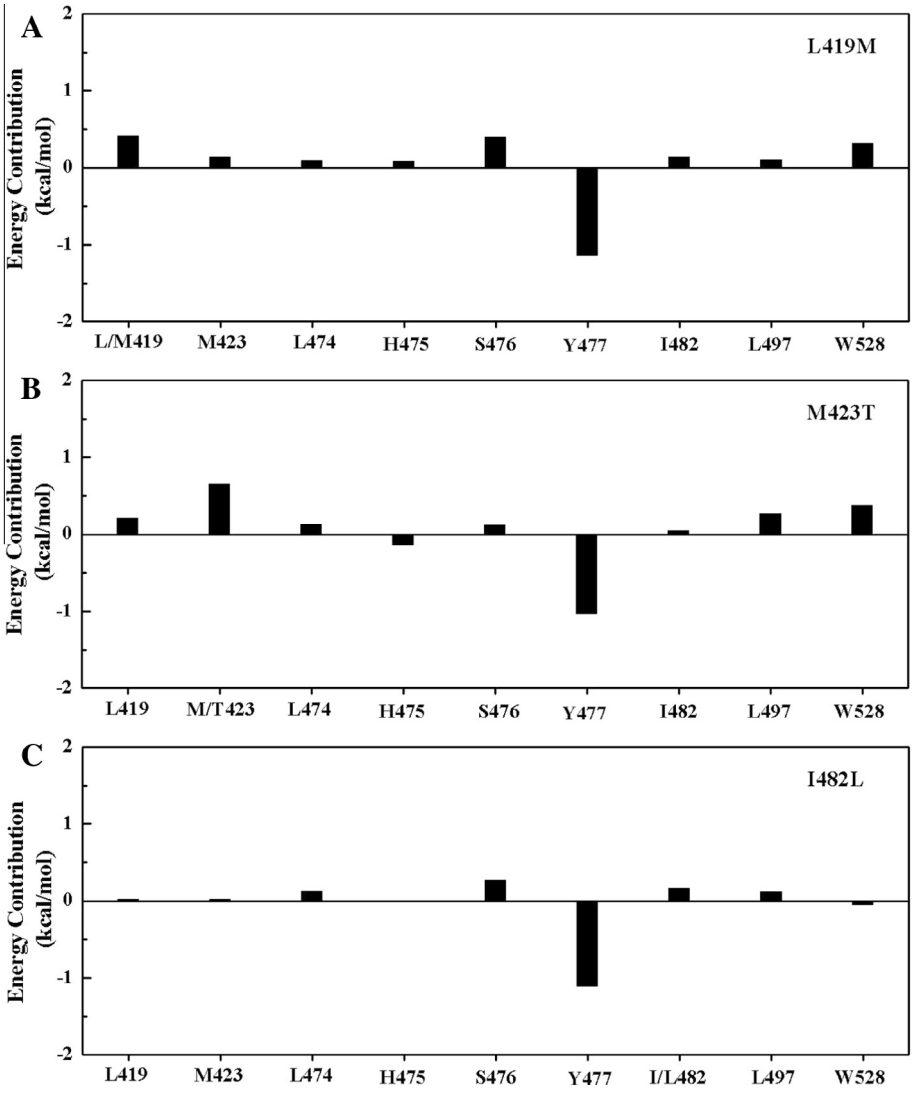

Fig. 8. The key residues contribution to the total binding free energy loss for VX-222 bound to the polymerase after mutations.

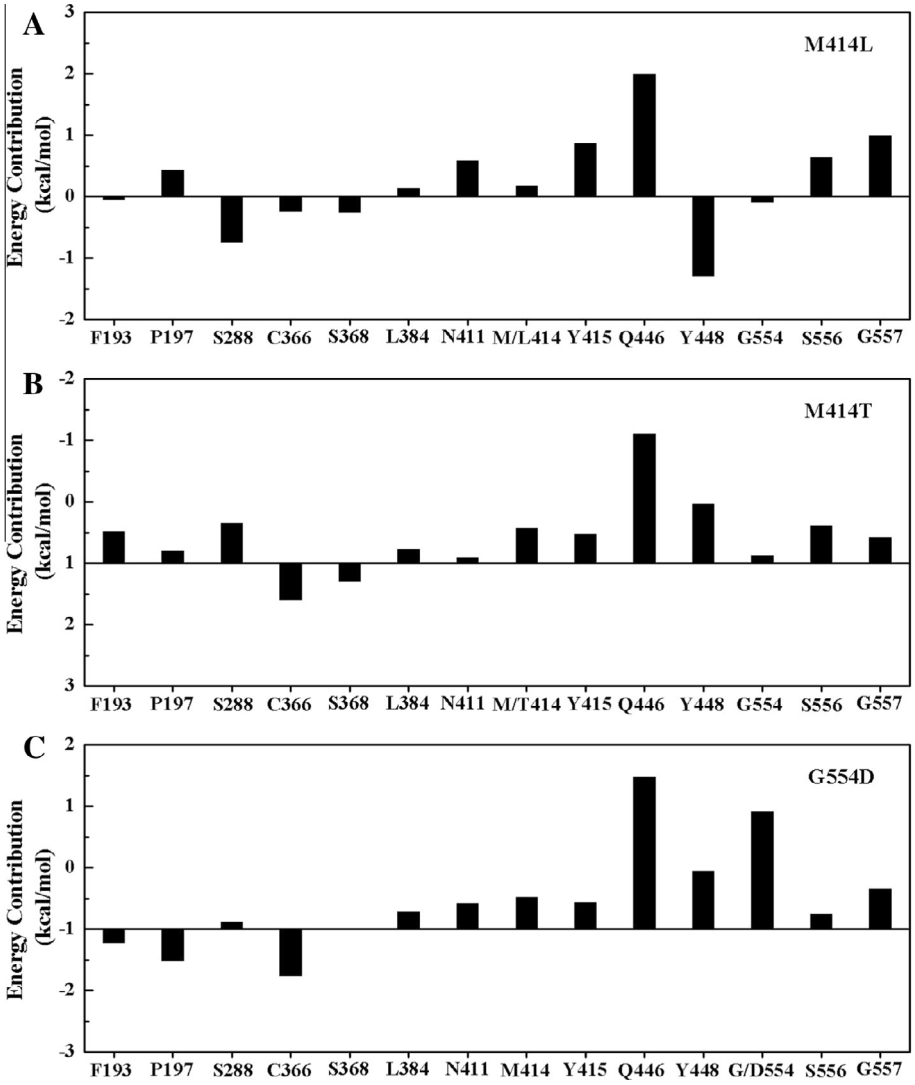

Fig. 9. The key residues contribution to the total binding free energy loss for ANA598 bound to the polymerase after mutations.

In the case of ANA598 bound three mutants models, the contribution from the residues L414, T414, and D554 are decreased by 0.18, 0.59, and 1.93 kcal/mol, respectively (Fig. 9). Furthermore, Supplementary Fig. S10 shown that the unfavorable shifts of L414 and T414 are mainly from the nonpolar interaction energy decreases, and the decreased interaction energy of D554 are mainly from the unfavorable polar contribution. Besides, the energy decomposition shown in Fig. 9 analysis suggests that other important residues (L384, N411, Y415, Q446, S556, and G557) are also involved in the favorable contribution loss of the binding of ANA598 caused by the drug resistance mutations. Among those residues, it is notable that Q446 exhibited significant unfavorable shifts in all mutant models (Fig. 9). Beside, a significant decrease of favorable interaction energies for the contributions from Y448 is only observed in the M414T and G554D mutants (Fig. 9). In Supplementary Fig. S10, it is apparent that the polar contribution of Q446 in all mutant models become more unfavorable compared with that in wild-type. Meanwhile, the unfavorable shift was examined for the nonpolar contribution of S288 and Y448 in M414T and G554D mutant models, and Q446 in all mutant models. In contrast, the M414L mutation causes an increase in the size of the nonpolar interaction energies for the S288 and Y448.

Supplementary Figs. S7 and S8 also indicate that, for all of the mutants, the drug resistance mutations do not occur on residues with maximal energetic contribution to the interaction. In addition, by comparing the energy contribution of the important residues in wild-type and mutant polymerase for VX-222 and ANA598 binding, it is apparent that each of the drug resistance mutation influences the interaction energies for the important residues (Supplementary Figs. S7 and S8), this is because of the indirect adjustments in the pockets (Fig. 4). For ANA598 bound complex, this could be explained by the fact that the palm I allosteric pocket overlaps with the enzyme active site. But for VX-222 bound thumb II allosteric pocket, that presumably should have greater freedom to mutate. Comparison of their energy contribution to the drug binding in wild-type complexes (Supplementary Figs. S7 and S8), it is found that the decreasing contribution to interaction (Figs. 8 and 9) may be related to the degree of conservation of these residues. It is interesting that in the studied systems, the residues that contribute most to the binding free energy are more conserved than others.

3.6. Understanding drug resistance mechanism through residue interaction network analysis

Several studies have shown that the residue interaction network (RIN) of protein structures have the small-world network properties (Böde et al., 2007; Vendruscolo et al., 2002;

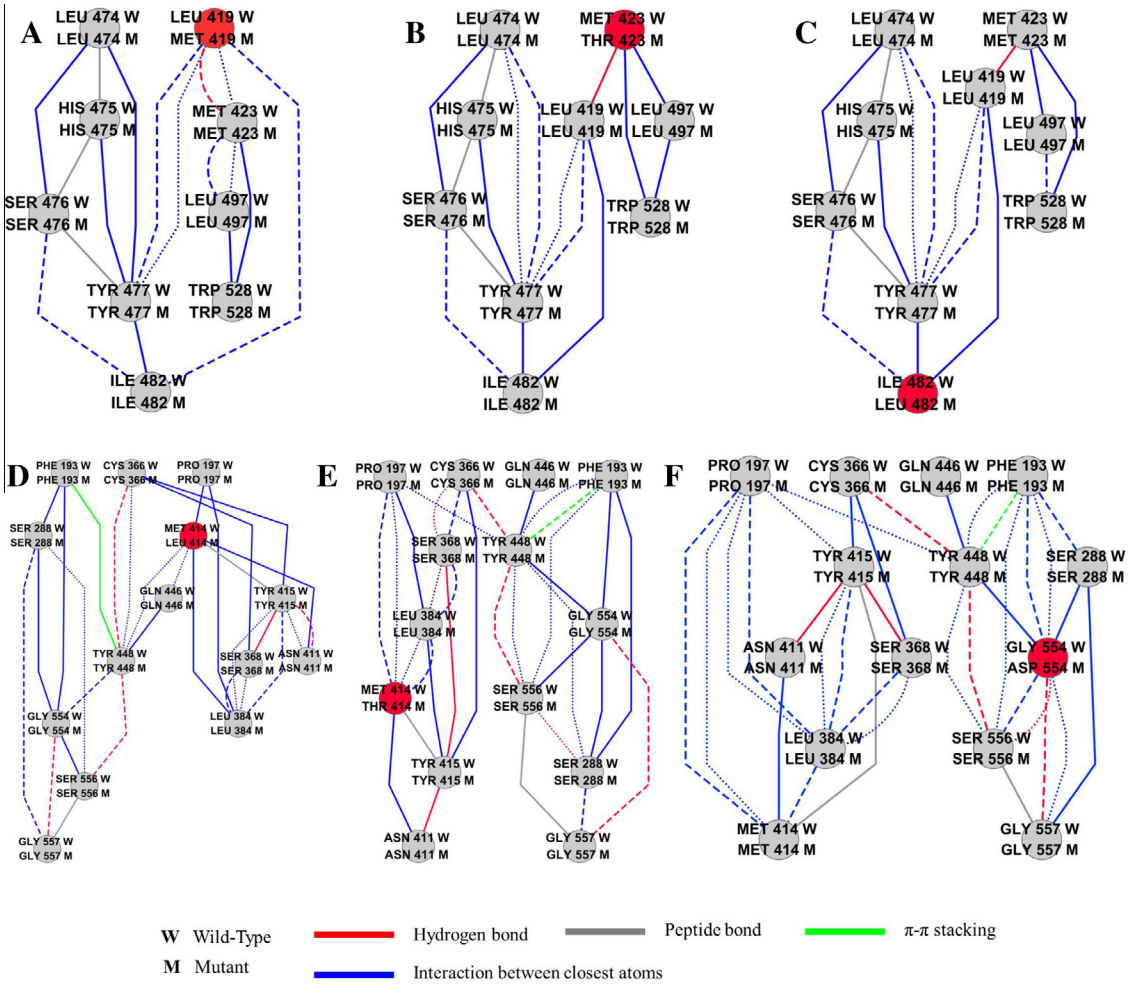

Fig. 10. The covalent and noncovalent interactions of the important residues for drug binding in the comparison network of VX-222 (A–C) and ANA598 (D–E) bound wild-type and mutant polymerase. Edge line styles correspond to noncovalent residue interactions that are preserved in both complex (solid lines), only in wild-type (dashed lines) or only in the mutant (dotted lines). The mutation residues are colored red and all other residues are in gray. (For interpretation of the references to color in this figure legend, the reader is referred to the web version of this article.)

Vishveshwara, 2009). Each amino acid residue in a protein structure is described as a node, and the noncovalent interactions between two nodes can be described as edges. Here, we attempted to further investigate the molecular mechanism of drug resistance to HCV NS5B polymerase mutants by analyzing the RIN of wild-type and mutant polymerase.

First, we calculated the RIN of wild-type and mutant polymerase by identifying all interactions between the amino acid residues. Then, we analyzed how drug resistance mutations influenced the RIN. Fig. 10 gave a detailed view of the comparison network of the most important residues for VX-222 and ANA598 binding to wild-type and mutant polymerase. It is obvious from the comparison networks that the noncovalent interactions of the residues are different in wild-type and mutant polymerase binding sites. For example, as shown in Fig. 10A, there are close atoms interactions between L419 and I482, S476 and I482 in the VX-222 bound wild-type polymerase, however, these interactions disappeared in the L419M mutant. In addition, L419 forms hydrogen bond interaction with M423 in wild-type polymerase, whereas this was replaced by the close atoms interactions between M419 and M423 in the M419 mutant (Fig. 10A). Likewise, in ANA598 bound polymerase, there are close atoms interactions between S288 and Gly557, Y448 and G554, hydrogen bond interactions between C366 and Y448, N411 and Y415, Y448 and S556, G554 and G557 in wild-type, but these interactions disappeared because of the M414L mutation (Fig. 10D). Meanwhile, Fig. 10D indicates that the close atoms interactions between N316 and Y448 were replaced by the hydrogen bond interactions in the M414L mutant. However, all these observed changes between the important residues shown in Fig. 10 may be critical to the drug resistance.

In addition, it is proposed that residues with highest betweenness and closeness centralities correspond to the conserved key residues that play the role of "hubs" in the RIN and these residues are critical to the protein structure and function (del Sol et al., 2006; Vendruscolo et al., 2002; Vishveshwara, 2009). In order to investigate the behavior of our calculated RIN, the topology properties including the shortest path betweenness and closeness centralities of the individual amino acid residue were characterized based on their relation with other residues of the polymerase. Interestingly, Figs. S11–S14 indicate that the mutant residues in the networks involved in the drug resistance possess a relatively lower size of the betweenness and closeness centralities. These findings are consistent with our recent network analysis of the residues outside the active site of HCV NS3/4A protease conferring drug resistance often with low topology centralities (Xue et al., 2013).

4. Conclusions

In the present study, we investigated the binding mode and resistance mechanism for wild-type and mutant HCV NS5B

polymerase to VX-222 and ANA598 through molecular modeling and residue interaction network analysis. Molecular docking calculations were applied to study the binding mode of VX-222 and ANA598 with HCV NS5B polymerase. Using MD simulations, the dynamic interaction between the drugs and polymerase as well as the corresponding conformational change caused by the drug resistant mutations were investigated. According to the calculated binding free energy, we found that, the studied mutations altered the binding mode of VX-222 and ANA598 and weakened the polymerase–drug interactions. In addition, decomposition of the binding free energy demonstrates that the mutations result in a decrease in the interaction energy for the most important residues which contribute to VX-222 and ANA598 binding. Finally, RIN analysis of wild-type and mutant protein structures indicate that the drug resistance mutation residues of the polymerase have a relatively low shortest path betweenness and closeness value in the network. All of these results clearly explain the effects that primary mutations in the binding pocket have on lowering VX-222 and ANA598 efficiency.

Acknowledgments

This work was supported by the National Natural Science Foundation of China (Grant No. 21175063) and the Program for Changjiang Scholars and Innovative Research Team in University (PCSIRT: IRT1137).

Appendix A. Supplementary data

Supplementary data associated with this article can be found, in the online version, at http://dx.doi.org/10.1016/j.antiviral.2014.01.006.

References

Adachi, T., Ago, H., Habuka, N., Okuda, K., Komatsu, M., Ikeda, S., Yatsunami, K., 2002. The essential role of C-terminal residues in regulating the activity of hepatitis C virus RNA-dependent RNA polymerase. Biochim. Biophys. Acta 1601, 38–48.

Alcaro, S., Artese, A., Ceccherini-Silberstein, F., Ortuso, F., Perno, C.F., Sing, T., Svicher, V., 2009. Molecular dynamics and free energy studies on the wild-type and mutated HIV-1 protease complexed with four approved drugs: mechanism of binding and drug resistance. J. Chem. Inf. Model. 49, 1751–1761.

Aruksakunwong, O., Wolschann, P., Hannongbua, S., Sompornpisut, P., 2006. Molecular dynamic and free energy studies of primary resistance mutations in HIV-1 protease–ritonavir complexes. J. Chem. Inf. Model. 46, 2085–2092.

Assenov, Y., Ramírez, F., Schelhorn, S.-E., Lengauer, T., Albrecht, M., 2008. Computing topological parameters of biological networks. Bioinformatics 24, 282–284.

Balius, T.E., Rizzo, R.C., 2009. Quantitative prediction of fold resistance for inhibitors of EGFR. Biochemistry 48, 8435–8448.

Bayly, C.I., Cieplak, P., Cornell, W., Kollman, P.A., 1993. A well-behaved electrostatic potential based method using charge restraints for deriving atomic charges: the RESP model. J. Phys. Chem. 97, 10269–10280.

Böde, C., Kovács, I.A., Szalay, M.S., Palotai, R., Korcsmáros, T., Csermely, P., 2007. Network analysis of protein dynamics. FEBS Lett. 581, 2776–2782.

Bressanelli, S., Tomei, L., Roussel, A., Incitti, I., Vitale, R.L., Mathieu, M., De Francesco, R., Rey, F.A., 1999. Crystal structure of the RNA-dependent RNA polymerase of hepatitis C virus. Proc. Natl. Acad. Sci. USA 96, 13034–13039.

Cai, Y., Schiffer, C.A., 2010. Decomposing the energetic impact of drug resistant mutations in HIV-1 protease on binding DRV. J. Chem. Theory Comput. 6, 1358–1368.

Caillet-Saguy, C., Simister, P.C., Bressanelli, S., 2011. An objective assessment of conformational variability in complexes of hepatitis C virus polymerase with non-nucleoside inhibitors. J. Mol. Biol. 414, 370–384.

Case, D.A., Darden, T.A., Cheatham III, T.E., Simmerling, C.L., Wang, J., Duke, R.E., Luo, R., Crowley, M., Walker, R.C., Zhang, W., Merz, K.M., Wang, B., Hayik, S., Roitberg, A., Seabra, G., Kolossváry, I., Wong, K.F., Paesani, F., Vanicek, J., Wu, X., Brozell, S.R., Steinbrecher, T., Gohlke, H., Yang, L., Tan, C., Mongan, J., Hornak, V., Cui, G., Mathews, D.H., Seetin, M.G., Sagui, C., Babin, V., Kollman, P.A., 2008. AMBER 10. University of California, San Francisco.

Chachra, R., Rizzo, R.C., 2008. Origins of resistance conferred by the R292K neuraminidase mutation via molecular dynamics and free energy calculations. J. Chem. Theory Comput. 4, 1526–1540.

Cieplak, P., Cornell, W.D., Bayly, C., Kollman, P.A., 1995. Application of the multimolecule and multiconformational RESP methodology to biopolymers: charge derivation for DNA, RNA, and proteins. J. Comput. Chem. 16, 1357–1377.

Darden, T., York, D., Pedersen, L., 1993. Particle mesh Ewald: an N·log(N) method for Ewald sums in large systems. J. Chem. Phys. 98, 10089–10092.

Davis, B.C., Thorpe, I.F., 2013. Thumb inhibitor binding eliminates functionally important dynamics in the hepatitis C virus RNA polymerase. Proteins 81, 40–52.

De Clercq, E., 2012. The race for interferon-free HCV therapies: a snapshot by the spring of 2012. Rev. Med. Virol. 22, 392–411.

del Sol, A., Fujihashi, H., Amoros, D., Nussinov, R., 2006. Residues crucial for maintaining short paths in network communication mediate signaling in proteins. Mol. Syst. Biol. 2 (2006), 0019.

D'Oliveira, A., Silva, C., De Souza, E., Andrade, L., Parana, R., Melo, R., 2009. Association between hepatitis C and hepatocellular carcinoma. J. Glob. Infect. Dis. 1, 33–37.

Doncheva, N.T., Klein, K., Domingues, F.S., Albrecht, M., 2011. Analyzing and visualizing residue networks of protein structures. Trends Biochem. Sci. 36, 179–182.

Duan, Y., Wu, C., Chowdhury, S., Lee, M.C., Xiong, G., Zhang, W., Yang, R., Cieplak, P., Luo, R., Lee, T., Caldwell, J., Wang, J., Kollman, P., 2003. A point-charge force field for molecular mechanics simulations of proteins based on condensed-phase quantum mechanical calculations. J. Comput. Chem. 24, 1999–2012.

Fox, T., Kollman, P.A., 1998. Application of the RESP methodology in the parametrization of organic solvents. J. Phys. Chem. B. 102, 8070–8079.

Freeman, L.C., 1978. Centrality in social networks conceptual clarification. Soc. Netw. 1, 215–239.

Fried, M.W., 2002. Side effects of therapy of hepatitis C and their management. Hepatology 36, s237–s244.

Fried, M.W., Shiffman, M.L., Reddy, K.R., Smith, C., Marinos, G., Gonçales, F.L., Häussinger, D., Diago, M., Carosi, G., Dhumeaux, D., Craxi, A., Lin, A., Hoffman, J., Yu, J., 2002. Peginterferon Alfa-2a plus ribavirin for chronic hepatitis C virus infection. N. Engl. J. Med. 347, 975–982.

Frisch, M.J., Trucks, G.W., Schlegel, H.B., Scuseria, G.E., Robb, M.A., Cheeseman, J.R., Scalmani, G., Barone, V., Mennucci, B., Petersson, G.A., Nakatsuji, H., Caricato, M., Li, X., Hratchian, H.P., Izmaylov, A.F., Bloino, J., Zheng, G., Sonnenberg, J.L., Hada, M., Ehara, M., Toyota, K., Fukuda, R., Hasegawa, J., Ishida, M., Nakajima, T., Honda, Y., Kitao, O., Nakai, H., Vreven, T., Montgomery Jr., J.A., Peralta, J.E., Ogliaro, F., Bearpark, M., Heyd, J.J., Brothers, E., Kudin, K.N., Staroverov, V.N., Kobayashi, R., Normand, J., Raghavachari, K., Rendell, A., Burant, J.C., Iyengar, S.S., Tomasi, J., Cossi, M., Rega, N., Millam, N.J., Klene, M., Knox, J.E., Cross, J.B., Bakken, V., Adamo, C., Jaramillo, J., Gomperts, R., Stratmann, R.E., Yazyev, O., Austin, A.J., Cammi, R., Pomelli, C., Ochterski, J.W., Martin, R.L., Morokuma, K., Zakrzewski, V.G., Voth, G.A., Salvador, P., Dannenberg, J.J., Dapprich, S., Daniels, A.D., Farkas, Ö., Foresman, J.B., Ortiz, J.V., Cioslowski, J., Fox, D.J., 2009. In Gaussian 09. Gaussian Inc., Wallingford, CT.

Guo, Z., Prongay, A., Tong, X., Fischmann, T., Bogen, S., Velazquez, F., Venkatraman, S., Njoroge, F.G., Madison, V., 2006. Computational study of the effects of mutations A156T, D168V, and D168Q on the binding of HCV protease inhibitors. J. Chem. Theory Comput. 2, 1657–1663.

Hadziyannis, S.J., Sette, J.H., Morgan, T.R., Balan, V., Diago, M., Marcellin, P., Ramadori, G., Bodenheimer, J.H., Bernstein, D., Rizzetto, M., Zeuzem, S., Pockros, P.J., Lin, A., Ackrill, A.M., 2004. Peginterferon-α2a and ribavirin combination therapy in chronic hepatitis CA randomized study of treatment duration and ribavirin dose. Ann. Intern. Med. 140, 346–355.

Hou, T., Yu, R., 2007. Molecular dynamics and free energy studies on the wild-type and double mutant HIV-1 protease complexed with amprenavir and two amprenavir-related inhibitors: mechanism for binding and drug resistance. J. Med. Chem. 50, 1177–1188.

Hou, T., McLaughlin, W.A., Wang, W., 2008. Evaluating the potency of HIV-1 protease drugs to combat resistance. Proteins 71, 1163–1174.

Hou, T., Zhang, W., Wang, J., Wang, W., 2009. Predicting drug resistance of the HIV-1 protease using molecular interaction energy components. Proteins 74, 837–846.

Jiao, P., Xue, W., Shen, Y., Jin, N., Liu, H., 2013. Understanding the drug resistance mechanism of hepatitis C virus NS5B to PF-00868554 due to mutations of 423 site: a computational study. Mol. Biosyst. http://dx.doi.org/10.1039/C3MB70498J.

Johnson, C.L., Gale, J.M., 2006. CARD games between virus and host get a new player. Trends Immunol. 27, 1–4.

Jorgensen, W.L., Chandrasekhar, J., Madura, J.D., Impey, R.W., Klein, M.L., 1983. Comparison of simple potential functions for simulating liquid water. J. Chem. Phys. 79, 926–935.

Kaminski, G.A., Friesner, R.A., Tirado-Rives, J., Jorgensen, W.L., 2001. Evaluation and reparametrization of the OPLS-AA force field for proteins via comparison with accurate quantum chemical calculations on peptides. J. Phys. Chem. B. 105, 6474–6487.

Kanda, T., Yokosuka, O., Omata, M., 2013. Treatment of hepatitis C virus infection in the future. Clin. Transl. Med. http://dx.doi.org/10.1186/2001-1326-2-9.

Kim, J.L., Morgenstern, K.A., Lin, C., Fox, T., Dwyer, M.D., Landro, J.A., Chambers, S.P., Markland, W., Lepre, C.A., O'Malley, E.T., Harbeson, S.L., Rice, C.M., Murcko, M.A., Caron, P.R., Thomson, J.A., 1996. Crystal structure of the hepatitis C virus NS3 protease domain complexed with a synthetic NS4A cofactor peptide. Cell 87, 343–355.

Kirkovsky, L., Zhou, Y., Shah, A., Tsan, M., LeBrun, L., Sergeeva, M., Norris, D., Bartkowski, D., Nolan, T., Khandurina, J., 2007. Preclinical characterization of a

novel, potent, and pharmacokinetically appealing nonnucleoside inhibitor of HCV NS5B polymerase. 58th Annu. Meet. Am. Assoc. Study Liver Dis.
Klibanov, O.M., Vickery, S.B., Olin, J.L., Smith, L.S., Williams, S.H., 2012. Boceprevir: a novel NS3/4 protease inhibitor for the treatment of hepatitis C. Pharmacotherapy 32, 173–190.
Kollman, P.A., Massova, I., Reyes, C., Kuhn, B., Huo, S., Chong, L., Lee, M., Lee, T., Duan, Y., Wang, W., Donini, O., Cieplak, P., Srinivasan, J., Case, D.A., Cheatham, T.E., 2000. Calculating structures and free energies of complex molecules: combining molecular mechanics and continuum models. Acc. Chem. Res. 33, 889–897.
Le Pogam, S., Kang, H., Harris, S.F., Leveque, V., Giannetti, A.M., Ali, S., Jiang, W.-R., Rajyaguru, S., Tavares, G., Oshiro, C., Hendricks, T., Klumpp, K., Symons, J., Browner, M.F., Cammack, N., Nájera, I., 2006. Selection and characterization of replicon variants dually resistant to thumb- and palm-binding nonnucleoside polymerase inhibitors of the hepatitis C virus. J. Virol. 80, 6146–6154.
Lesburg, C.A., Cable, M.B., Ferrari, E., Hong, Z., Mannarino, A.F., Weber, P.C., 1999. Crystal structure of the RNA-dependent RNA polymerase from hepatitis C virus reveals a fully encircled active site. Nat. Struct. Mol. Biol. 6, 937–943.
Li, L., Li, Y., Zhang, L., Hou, T., 2012. Theoretical studies on the susceptibility of oseltamivir against variants of 2009 A/H1N1 influenza neuraminidase. J. Chem. Inf. Model. 52, 2715–2729.
Liu, H., Yao, X., Wang, C., Han, J., 2010. In silico identification of the potential drug resistance sites over 2009 influenza A (H1N1) virus neuraminidase. Mol. Pharm. 7, 894–904.
Lohmann, V., 2013. Hepatitis C virus RNA replication. In: Bartenschlager, R. (Ed.), Hepatitis C Virus: From Molecular Virology to Antiviral Therapy. Springer, Berlin Heidelberg, pp. 167–198.
Love, R.A., Parge, H.E., Wickersham, J.A., Hostomsky, Z., Habuka, N., Moomaw, E.W., Adachi, T., Hostomska, Z., 1996. The crystal structure of hepatitis C virus NS3 proteinase reveals a trypsin-like fold and a structural zinc binding site. Cell 87, 331–342.
Massova, I., Kollman, P., 2000. Combined molecular mechanical and continuum solvent approach (MM-PBSA/GBSA) to predict ligand binding. Perspect. Drug Discov. 18, 113–135.
Matthews, S.J., Lancaster, J.W., 2012. Telaprevir: a hepatitis C NS3/4A protease inhibitor. Clin. Ther. 34, 1857–1882.
Melnikova, I., 2011. Hepatitis C – pipeline update. Nat. Rev. Drug Discov. 10, 93–94.
Ontoria, J.M., Rydberg, E.H., Di Marco, S., Tomei, L., Attenni, B., Malancona, S., Martin Hernando, J.I., Gennari, N., Koch, U., Narjes, F., Rowley, M., Summa, V., Carroll, S.S., Olsen, D.B., De Francesco, R., Altamura, S., Migliaccio, G., Carfi, A., 2009. Identification and biological evaluation of a series of 1H-benzo[de]isoquinoline-1,3(2H)-diones as hepatitis C virus NS5B polymerase inhibitors. J. Med. Chem. 52, 5217–5227.
Onufriev, A., Bashford, D., Case, D.A., 2000. Modification of the generalized born model suitable for macromolecules. J. Phys. Chem. B. 104, 3712–3720.
Pan, D., Sun, H., Bai, C., Shen, Y., Jin, N., Liu, H., Yao, X., 2011. Prediction of zanamivir efficiency over the possible 2009 influenza A (H1N1) mutants by multiple molecular dynamics simulations and free energy calculations. J. Mol. Model. 17, 2465–2473.
Pan, D., Xue, W., Zhang, W., Liu, H., Yao, X., 2012. Understanding the drug resistance mechanism of hepatitis C virus NS3/4A to ITMN-191 due to R155K, A156V, D168A/E mutations: a computational study. Biochim. Biophys. Acta 1820, 1526–1534.
Pearlman, D.A., Case, D.A., Caldwell, J.W., Ross, W.S., Cheatham Iii, T.E., DeBolt, S., Ferguson, D., Seibel, G., Kollman, P., 1995. AMBER, a package of computer programs for applying molecular mechanics, normal mode analysis, molecular dynamics and free energy calculations to simulate the structural and energetic properties of molecules. Comput. Phys. Commun. 91, 1–41.
Rizzo, R.C., Toba, S., Kuntz, I.D., 2004. A molecular basis for the selectivity of thiadiazole urea inhibitors with stromelysin-1 and gelatinase-A from generalized born molecular dynamics simulations. J. Med. Chem. 47, 3065–3074.
Rocchia, W., Alexov, E., Honig, B., 2001. Extending the applicability of the nonlinear poisson−boltzmann equation: multiple dielectric constants and multivalent ions. J. Phys. Chem. B. 105, 6507–6514.
Ruebsam, F., Murphy, D.E., Tran, C.V., Li, L.-S., Zhao, J., Dragovich, P.S., McGuire, H.M., Xiang, A.X., Sun, Z., Ayida, B.K., Blazel, J.K., Kim, S.H., Zhou, Y., Han, Q., Kissinger, C.R., Webber, S.E., Showalter, R.E., Shah, A.M., Tsan, M., Patel, R.A., Thompson, P.A., LeBrun, L.A., Hou, H.J., Kamran, R., Sergeeva, M.V., Bartkowski, D.M., Nolan, T.G., Norris, D.A., Khandurina, J., Brooks, J., Okamoto, E., Kirkovsky, L., 2009. Discovery of tricyclic 5,6-dihydro-1H-pyridin-2-ones as novel, potent, and orally bioavailable inhibitors of HCV NS5B polymerase. Bioorg. Med. Chem. Lett. 19, 6404–6412.
Ryckaert, J.-P., Ciccotti, G., Berendsen, H.J.C., 1977. Numerical integration of the cartesian equations of motion of a system with constraints: molecular dynamics of *n*-alkanes. J. Comput. Phys. 23, 327–341.
Schrödinger, 2009a. Maestro, Version 9.0. Schrödinger LLC, New York, NY.
Schrödinger, 2009b. LigPrep, Version 2.3. Schrödinger LLC, New York, NY.
Schrödinger, 2009c. Epik, Version 2.0. Schrödinger LLC, New York, NY.
Schrödinger, 2009d. Prime Version 2.1. Schrödinger LLC, New York, NY.
Schrödinger, 2009e. Glide, Version 5.5. Schrödinger LLC, New York, NY.
Shannon, P., Markiel, A., Ozier, O., Baliga, N.S., Wang, J.T., Ramage, D., Amin, N., Schwikowski, B., Ideker, T., 2003. Cytoscape: a software environment for integrated models of biomolecular interaction networks. Genome Res. 13, 2498–2504.
Sitkoff, D., Sharp, K.A., Honig, B., 1994. Accurate calculation of hydration free energies using macroscopic solvent models. J. Phys. Chem. 98, 1978–1988.
Sofia, M.J., Chang, W., Furman, P.A., Mosley, R.T., Ross, B.S., 2011. Nucleoside, nucleotide, and non-nucleoside inhibitors of hepatitis C virus NS5B RNA-dependent RNA-polymerase. J. Med. Chem. 55, 2481–2531.
Soriano, V., Vispo, E., de Mendoza, C., Labarga, P., Fernandez-Montero, J.V., Poveda, E., Treviño, A., Barreiro, P., 2013. Hepatitis C therapy with HCV NS5B polymerase inhibitors. Expert Opin. Pharmacother. 14, 1161–1170.
Stoica, I., Sadiq, S.K., Coveney, P.V., 2008. Rapid and accurate prediction of binding free energies for saquinavir-bound HIV-1 proteases. J. Am. Chem. Soc. 130, 2639–2648.
Tellinghuisen, T.L., Marcotrigiano, J., Rice, C.M., 2005. Structure of the zinc-binding domain of an essential component of the hepatitis C virus replicase. Nature 435, 374–379.
Tsui, V., Case, D.A., 2000. Theory and applications of the generalized born solvation model in macromolecular simulations. Biopolymers 56, 275–291.
Vendruscolo, M., Dokholyan, N.V., Paci, E., Karplus, M., 2002. Small-world view of the amino acids that play a key role in protein folding. Phys. Rev. E 65, 061910.
Vergara-Jaque, A., Poblete, H., Lee, E.H., Schulten, K., González-Nilo, F., Chipot, C., 2012. Molecular basis of drug resistance in A/H1N1 virus. J. Chem. Inf. Model. 52, 2650–2656.
Vishveshwara, S., 2009. Intra and inter-molecular communications through protein structure. Curr. Protein Pept. Sci. 10, 146–160.
Wang, J., Wolf, R.M., Caldwell, J.W., Kollman, P.A., Case, D.A., 2004. Development and testing of a general amber force field. J. Comput. Chem. 25, 1157–1174.
Welsch, C., Domingues, F., Susser, S., Antes, I., Hartmann, C., Mayr, G., Schlicker, A., Sarrazin, C., Albrecht, M., Zeuzem, S., Lengauer, T., 2008. Molecular basis of telaprevir resistance due to V36 and T54 mutations in the NS3-4A protease of the hepatitis C virus. Genome Biol. 9, R16.
Welsch, C., Schweizer, S., Shimakami, T., Domingues, F.S., Kim, S., Lemon, S.M., Antes, I., 2012. Ketoamide resistance and hepatitis C virus fitness in Val55 variants of the NS3 serine protease. Antimicrob. Agents Chemother. 56, 1907–1915.
Word, J.M., Lovell, S.C., LaBean, T.H., Taylor, H.C., Zalis, M.E., Presley, B.K., Richardson, J.S., Richardson, D.C., 1999a. Visualizing and quantifying molecular goodness-of-fit: small-probe contact dots with explicit hydrogen atoms. J. Mol. Biol. 285, 1711–1733.
Word, J.M., Lovell, S.C., Richardson, J.S., Richardson, D.C., 1999b. Asparagine and glutamine: using hydrogen atom contacts in the choice of side-chain amide orientation. J. Mol. Biol. 285, 1735–1747.
Xue, W., Jin, X., Ning, L., Wang, M., Liu, H., Yao, X., 2012a. Exploring the molecular mechanism of cross-resistance to HIV-1 integrase strand transfer inhibitors by molecular dynamics simulation and residue interaction network analysis. J. Chem. Inf. Model. 53, 210–222.
Xue, W., Wang, M., Jin, X., Liu, H., Yao, X., 2012b. Understanding the structural and energetic basis of inhibitor and substrate bound to the full-length NS3/4A: insights from molecular dynamics simulation, binding free energy calculation and network analysis. Mol. Biosyst. 8, 2753–2765.
Xue, W., Ban, Y., Liu, H., Yao, X., 2013. Computational study on the drug resistance mechanism against HCV NS3/4A protease inhibitors vaniprevir and MK-5172 by the combination use of molecular dynamics simulation, residue interaction network, and substrate envelope analysis. J. Chem. Inf. Model. http://dx.doi.org/10.1021/ci400060j.
Yao, N., Reichert, P., Taremi, S.S., Prosise, W.W., Weber, P.C., 1999. Molecular views of viral polyprotein processing revealed by the crystal structure of the hepatitis C virus bifunctional protease–helicase. Structure 7, 1353–1363.
Yi, G., Deval, J., Fan, B., Cai, H., Soulard, C., Ranjith-Kumar, C.T., Smith, D.B., Blatt, L., Beigelman, L., Kao, C.C., 2012. Biochemical study of the comparative inhibition of hepatitis C virus RNA polymerase by VX-222 and filibuvir. Antimicrob. Agents Chemother. 56, 830–837.
Yoon, J., Blumer, A., Lee, K., 2006. An algorithm for modularity analysis of directed and weighted biological networks based on edge-betweenness centrality. Bioinformatics 22, 3106–3108.
Zhang, J., Hou, T., Wang, W., Liu, J.S., 2010. Detecting and understanding combinatorial mutation patterns responsible for HIV drug resistance. Proc. Natl. Acad. Sci. USA 107, 1321–1326.
Zhou, Z., Madrid, M., Evanseck, J.D., Madura, J.D., 2005. Effect of a bound non-nucleoside RT inhibitor on the dynamics of wild-type and mutant HIV-1 reverse transcriptase. J. Am. Chem. Soc. 127, 17253–17260.